Direct and inverse scattering in the time domain for a dissipative wave equation. II. Simultaneous reconstruction of dissipation and phase velocity profiles

G. Kristensson
Division of Electromagnetic Theory, Royal Institute of Technology, S-100 44 Stockholm, Sweden

R. J. Krueger
Applied Mathematical Sciences, Ames Laboratory—United States Department of Energy, Iowa State University, Ames, Iowa 50011

(Received 8 August 1985; accepted for publication 30 January 1986)

The one-dimensional inverse scattering problem for inhomogeneous lossy media is considered. The model problem involves electromagnetic wave propagation in a medium of unknown thickness with spatially varying conductivity and permittivity. Two inversion algorithms are developed in the time domain using data obtained from normally incident plane waves. These algorithms utilize reflection data from both sides of the medium, and one of them also uses transmission data. These algorithms are implemented numerically on several examples, one of which includes the effects of noisy data. The possibility of using one-sided reflection data and no transmission data is reviewed and analyzed.

I. INTRODUCTION

Inverse scattering problems for lossy media are not well understood, even in the one-dimensional case. Such problems can be addressed on a variety of levels, depending on the underlying model of dissipation and the information sought from the inversion procedure. In this paper a one-dimensional wave propagation model is considered in which the dissipation and phase velocity are spatially varying functions; i.e., functions of depth in the medium. The analysis is carried out in the time domain. Inversion procedures are developed for simultaneously reconstructing the dissipation and phase velocity profiles using data obtained from normally incident plane waves.

In a previous paper[1] (hereafter called Part I) various aspects of the direct scattering problem were developed. The pertinent results from Part I will be summarized in Sec. II below. Hence, the reader who is primarily interested in the inverse problem will find this paper fairly self-contained, with the exception that the first two sections of Part I should be consulted for an overview of the problem at hand and also for an explanation of the notation.

A model problem for the techniques presented here involves one-dimensional electromagnetic wave propagation in a medium characterized by nonconstant permittivity and conductivity profiles. A precise statement of the model problem is given in Part I, Sec. II.

Two inversion algorithms are developed in this paper. In both of them it is assumed that the medium has finite but unknown thickness and that reflection data are available on both sides of the medium. One of the algorithms also requires transmission data. All of these data are in the form of finite time traces of impulse responses. The specific data requirements are given in Sec. III.

The inversion procedure using transmission data and both sets of reflection data is shown in Sec. III. Two numerical examples are also given, one of which shows the performance of the algorithm using noisy data. In Sec. IV the inversion algorithm using only reflection data is given. This is an iteration procedure, and a numerical example of its performance is also provided. In Sec. V the question of inverting reflection data from only one side of the medium is considered. Inversions of this nature have been addressed in previous works[2,3] under the assumption that either the conductivity or permittivity is known *a priori*. In the present paper, it is shown that if only a finite time trace of the (reflected) impulse response is known, and no information regarding the medium is given, then an infinite number of medium profiles can be found that produce such a time trace.

A number of authors[4–8] have developed inversion procedures for dissipative media that require two-sided reflection data as well as transmission data. The inversion procedure given in Sec. III seems to be more intuitive than these other procedures since it clearly shows the interplay between the early time behavior of one reflected signal with the late time behavior of the reflected signal from the other side. This is also evident in the inversion procedure in Sec. IV. An inversion procedure using transmission data and one-sided reflection data has been previously developed,[9–11] although the model problem is different from that considered in this paper.

A brief summary is presented in Sec. VI. Also, an example is provided that demonstrates that under certain conditions it is possible for two different media to produce the same two-sided reflection data for time traces corresponding to one round trip in the medium.

The paper concludes with an Appendix that provides sufficient conditions for the inversion procedure of Sec. IV to be well posed.

II. SUMMARY OF PREVIOUS RESULTS

The equations used in the inverse algorithms presented in this paper are summarized in this section. The reader interested in the details in the derivations is referred to Part I.

The reflection kernels $R^{\pm}(x,y,s)$ for the subregion

 0022-2488/86/061683-11$02.50

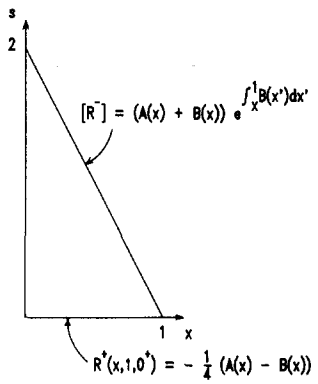

FIG. 1. The domain of $R^+(x,1,s)$ for one round trip. The boundary value of R^+ at $s=0^+$ and the discontinuity of R^- along the line $s=2(1-x)$ are also shown.

$[x,y]$ satisfy (see also Sec. III, Part I)

$$R_x^+(x,y,s) = 2R_s^+(x,y,s) - B(x)R^+(x,y,s) - \tfrac{1}{2}[A(x)+B(x)] \times \int_0^s R^+(x,y,s')R^+(x,y,s-s')ds', \quad s>0, \tag{2.1}$$

$$R^+(x,y,0^+) = -\tfrac{1}{4}[A(x)-B(x)], \quad x<y,$$

$$R_y^-(x,y,s) = -2R_s^-(x,y,s) + B(y)R^-(x,y,s) - \tfrac{1}{2}[A(y)-B(y)] \times \int_0^s R^-(x,y,s')R^-(x,y,s-s')ds', \quad s>0, \tag{2.2}$$

$$R^-(x,y,0^+) = \tfrac{1}{4}[A(y)+B(y)], \quad x<y.$$

These kernels are discontinuous across the plane $s=2(y-x)$. The discontinuities can be related to the internal properties of the slab (see Fig. 1):

$$[R^+(x,y,s)]_{s=2(y-x)^-}^{s=2(y-x)^+} = \tfrac{1}{4}[A(y)-B(y)]\exp\left\{\int_x^y B(x')dx'\right\}, \tag{2.3}$$

$$[R^-(x,y,s)]_{s=2(y-x)^-}^{s=2(y-x)^+} = -\tfrac{1}{4}[A(x)+B(x)]\exp\left\{\int_x^y B(x')dx'\right\}.$$

Furthermore, the kernels satisfy

$$R^+(x,y,s) = R^+(x,x+s/2^+,s), \quad s<2(y-x),$$
$$R^-(x,y,s) = R^-(y-s/2^-,y,s), \quad s<2(y-x). \tag{2.4}$$

These last relations express the property that the reflected field is independent of position of the rear interface for times less than one round trip.

In Sec. III in Part I, the effect of reciprocity on the transmission kernels $T^\pm(x,y,s)$ was analyzed. It was shown that the two transmission kernels $T^\pm(x,y,s)$ are proportional to each other as functions of s, as are the propagator kernels $W^\pm(x,y,s)$. Thus it suffices to consider just one transmission kernel T and one propagator kernel W. The relations are

$$T(x,y,s) = T^+(x,y,s)/t^+(x,y) = T^-(x,y,s)/t^-(x,y), \tag{2.5}$$

$$W(x,y,s) = W^+(x,y,s)t^+(x,y) = W^-(x,y,s)t^-(x,y), \tag{2.6}$$

where

$$t^\pm(x,y) = \exp\left\{\mp\frac{1}{2}\int_x^y [A(x') \mp B(x')]dx'\right\}. \tag{2.7}$$

The resolvent equation which relates T and W to each other is

$$T(x,y,s) + W(x,y,s) + \int_0^s T(x,y,s-s')\,W(x,y,s')ds' = 0. \tag{2.8}$$

The propagator kernel W satisfies the imbedding equations

$$W_x(x,y,s) = \frac{1}{2}[A(x)+B(x)]\left\{R^+(x,y,s) + \int_0^s W(x,y,s')R^+(x,y,s-s')ds'\right\}, \quad s>0, \tag{2.9}$$

$$W_y(x,y,s) = \frac{1}{2}[A(y)-B(y)]\left\{R^-(x,y,s) + \int_0^s W(x,y,s')R^-(x,y,s-s')ds'\right\}, \quad s>0. \tag{2.10}$$

In Sec. V in Part I the extension of data from one round trip, $0<s<2(y-x)$, to arbitrary time s is derived. Transmission data and reflection data for $0<s<2(y-x)$ are extended to $s>2(y-x)$ by the following equations:

$$T(x,y,s) + \int_{2(y-x)}^s W(x,y,s-s')T(x,y,s')ds' = G(x,y,s) = \begin{cases} -\displaystyle\int_{s-2(y-x)}^{2(y-x)} W(x,y,s-s')T(x,y,s')ds', & 2(y-x)<s<4(y-x), \\ 0, & s>4(y-x), \end{cases} \tag{2.11}$$

$$R^\pm(x,y,s) = \int_0^{2(y-x)} T(x,y,s-s')\left[R^\pm(x,y,s') + \int_0^{s'} W(x,y,s'-s'')R^\pm(x,y,s'')ds''\right]ds', \quad s>2(y-x). \tag{2.12}$$

III. THE INVERSION ALGORITHM WITH COMPLETE DATA

The new algorithm presented in this section utilizes a complete set of data, namely the two (physical) reflection kernels $R^{\pm}(0,1,s)$ and the (physical) transmission kernel $T(0,1,s)$ for a complete round trip in the slab, $0<s<2$. These data are complete in the sense that they can be extended to arbitrary time s by the extension procedure described in Sec. V in Part I. Loosely speaking, the algorithm combines an early time behavior in $R^{\pm}$ with a late time behavior in $R^{\mp}$ and the properties of the discontinuity in $R^{\mp}$. This statement and its more precise meaning will become much clearer in this section.

All the data described above and the constant $G(1)$ defined below are needed to recover the two unknown functions $A(x)$ and $B(x)$, $0<x<1$. From these two functions it is then easy to find the unknown permittivity and conductivity as a function of z as well as the total length L of the slab. However, two more constants are needed to transform from A and B to ϵ and σ. Thus the complete set of data to simultaneously recover both the permittivity and the conductivity are

$$\begin{aligned} &R^{+}(0,1,s), \quad 0<s<2,\\ &R^{-}(0,1,s), \quad 0<s<2,\\ &T(0,1,s), \quad 0<s<2,\\ &G(1),\\ &l,\\ &\epsilon(0) \quad \text{or} \quad \epsilon(L), \end{aligned} \tag{3.1}$$

where

$$\begin{aligned} G(x) &= 1/[t^{+}(0,x)t^{-}(0,x)]\\ &= \exp\left\{-\int_0^x B(x')\right\}dx' \end{aligned}$$

[see Eq. (2.7) for a definition of $t^{\pm}(x,y)$], and $G(1)$ is a constant associated with the attenuation of the field within the slab. From the definition of the transmission operators [Eqs. (2.18) and (2.20) in Part I], $G(1)$ is a measurable quantity. The constant l [see Eq. (2.6) in Part I] is a constant related to the total time of measurement. The permittivity $\epsilon(0)$ at the left interface [or $\epsilon(L)$ at the right] is also assumed to be known from experimental data.

The inversion algorithm works from one side of the medium to the other. For convenience the algorithm is presented for a propagation from the left-hand side of the slab towards the right and all the details of the alogorithm will be shown for this particular choice. Thus, the subregions to be considered are of the form $[x,1]$ with y being fixed at 1. The necessary modifications to propagate from the right-hand side are rather straightforward.

In Eq. (2.3), the jump across the plane $s=2(y-x)$ was given as a function of the internal properties of the slab. This jump can, however, be expressed in an alternative way by the extension of data presented in Sec. V in Part I. Suppose the reflection data are known for $s<2(y-x)$. In terms of these data the value just above the plane $s=2(y-x)$ can be calculated from Eq. (2.12). The resulting jump is

$$\begin{aligned} &[R^{\pm}(x,y,s)]_{s=2(y-x)^{-}}^{s=2(y-x)^{+}}\\ &\quad=\int_0^{2(y-x)} T(x,y,2(y-x)-s')\left[R^{\pm}(x,y,s')\right.\\ &\qquad\left.+\int_0^{s'} W(x,y,s'-s'')R^{\pm}(x,y,s'')ds''\right]ds'\\ &\qquad-R^{\pm}(x,y,2(y-x)^{-})\\ &\quad=-\int_0^{2(y-x)} W(x,y,2(y-x)-s')R^{\pm}(x,y,s')ds'\\ &\qquad-R^{\pm}(x,y,2(y-x)^{-}). \end{aligned} \tag{3.2}$$

The resolvent equation, Eq. (2.8), has been used to simplify the expression above. In particular, the jump in the reflection kernel R^{-} for $y=1$ can, with use of Eq. (2.4), be expressed as

$$\begin{aligned} &[R^{-}(x,1,s)]_{s=2(1-x)^{-}}^{s=2(1-x)^{+}}\\ &\quad=-\int_0^{2(1-x)} W(x,1,2(1-x)-s')R^{-}(0,1,s')ds'\\ &\qquad-R^{-}(0,1,2(1-x)^{-}). \end{aligned} \tag{3.3}$$

It should be noted that only the physical kernel $R^{-}(0,1,s)$, $0<s<2$, is used in Eq. (3.3).

From the equations above it is now clear that knowing $R^{\pm}(x,1,s)$ and $W(x,1,s)$ for a fixed x gives two linearly independent relations between the two unknown functions $A(x)$ and $B(x)$ at the point x. This can be seen by combining Eqs. (2.3) and (3.3) together with the early time behavior of $R^{+}(x,1,s)$ in Eq. (2.1),

$$\begin{aligned} &\int_0^{2(1-x)} W(x,1,2(1-x)-s')R^{-}(0,1,s')ds'\\ &\qquad+R^{-}(0,1,2(1-x)^{-})\\ &\quad=\frac{1}{4}[A(x)+B(x)]\exp\left\{\int_x^1 B(x')dx'\right\},\\ &R^{+}(x,1,0^{+})=-\tfrac{1}{4}[A(x)-B(x)]. \end{aligned} \tag{3.4}$$

Before describing the general inversion algorithm, the initialization of the procedure is addressed. From the data in Eq. (3.1) the resolvent $W(0,1,s)$, $0<s<2$, is obtained by solving Eq. (2.8) at $x=0$. Equations (3.4) are then easily solved for $A(x)$ and $B(x)$ at $x=0^{+}$ and the initialization of $A(x)$ and $B(x)$ is completed.

The inversion scheme can now be written down in a general setting. As in earlier works,[2,12] which used only the R^{+} equation [Eq. (2.1)], a grid of points is established in (x,s) space. The mesh is uniform in each direction, with $\Delta s=2\Delta x$, which takes advantage of the directional derivative nature of Eq. (2.1). Now Eqs. (2.1) and (2.9) are discretized on this grid. The calculation proceeds from left to right across the grid, starting at $x=0$ and marching to $x=1$, with $0\leqslant s\leqslant 2(1-x)$. In its most basic form, the inversion algorithm for determining $A(x)$ and $B(x)$ is as follows.

(1) Equation (2.9) is used to explicitly step $W(x,1,s)$ forward in the x direction to the next set of x grid points.

(2) Equation (2.1) is used to implicitly step a portion of $R^{+}(x,1,s)$ forward in the x direction to the next x grid point at $s=0$.

(3) Equations (3.4) are used at these new x grid points to obtain $A(x)$ and $B(x)$.

(4) Equation (2.1) is used to implicitly step the remaining $R^{+}(x,1,s)$ data forward in the x direction to the next set of x grid points.

(5) Now repeat steps (1) through (4) to move one step deeper into the slab.

This procedure can be modified in a number of ways to improve its numerical accuracy. Details regarding the numerical implementation are not discussed here.

There are some interesting points to notice in the inversion algorithm outlined above. First, the transmission data $T(0,1,s)$ are used only in the initialization step, and thereafter it is the resolvent of T that is used to step into the medium. Second, since the calculation is being carried out in the plane $y=1$ (see Part I, Fig. 4), the $R^{-}(0,1,s)$ data are constant on lines of constant s. Therefore, it is not necessary to propagate R^{-} into the medium via an integrodifferential equation; rather, it is the physical data $R^{-}(0,1,s)$ that appears in Eq. (3.4).

The final step in the inversion scheme is to calculate the depth $z(x)$, the total length L, the permittivity $\epsilon(z)$, and the conductivity $\sigma(z)$ from the profile functions $A(x)$ and $B(x)$, $0<x<1$. From the definitions of $A(x)$ and $B(x)$, given by Eqs. (2.15) and (2.16) in Part I, it is easy to obtain the following relations:

$$z(x)=\frac{l}{\sqrt{\mu_0\epsilon(0)}}\int_0^x \exp\left[-\int_0^{x'} A(x'')dx''\right]dx', \quad 0<x<1, \tag{3.5}$$

$$\epsilon(z(x))=\epsilon(0)\exp\left[2\int_0^x A(x')dx'\right], \tag{3.6}$$

$$\sigma(z(x))=\frac{-\epsilon(0)B(x)\exp\left[2\int_0^x A(x')dx'\right]}{l}. \tag{3.7}$$

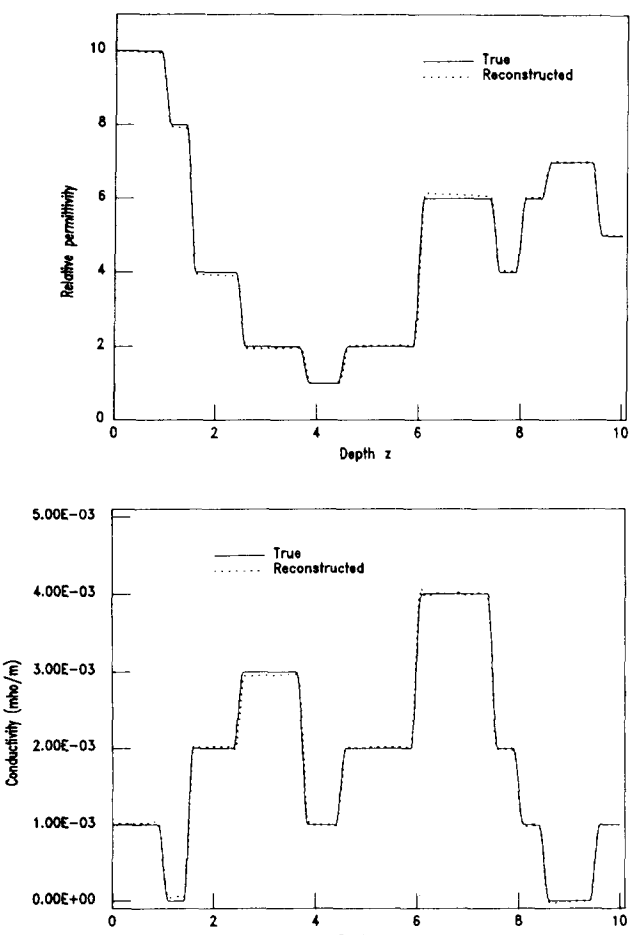

FIG. 2. The relative permittivity and conductivity profiles in example 1. The depth is given in m.

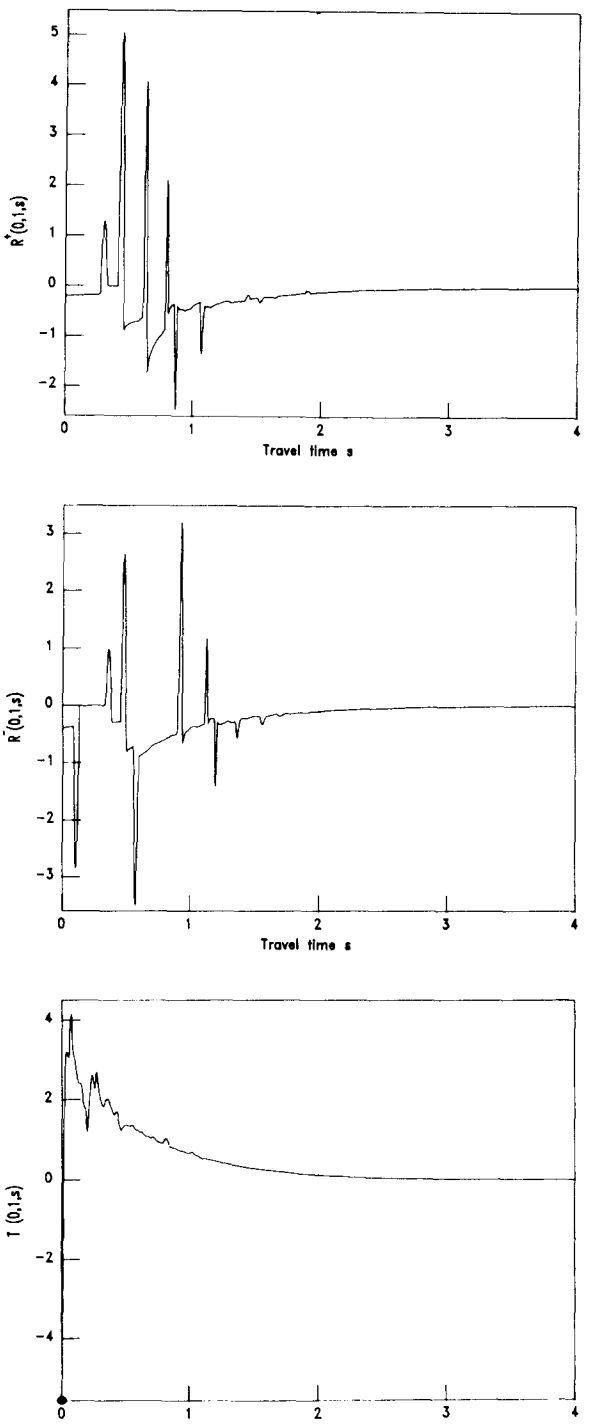

FIG. 3. The physical scattering kernels $R^{\pm}(0,1,s)$ and $T(0,1,s)$ for example 1. Two round trips are shown. The value of $T(0,1,0^{+})$ is marked with a solid dot.

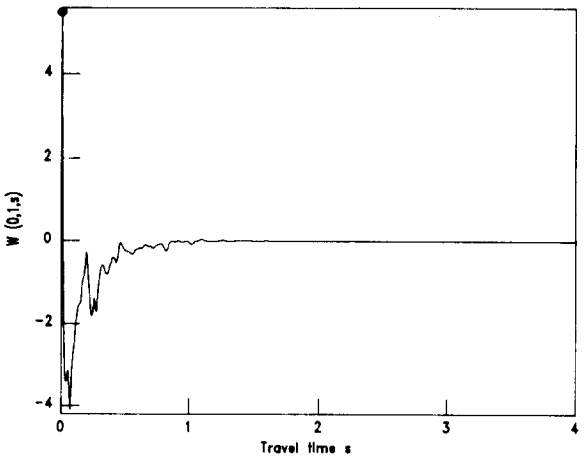

FIG. 4. The resolvent kernel $W(0,1,s)$ for example 1. Two round trips are shown. The value of $W(0,1,0^+)$ is marked with a solid dot.

In particular, the total length L of the slab is

$$L = \frac{l}{\sqrt{\mu_0 \epsilon(0)}} \int_0^1 \exp\left[-\int_0^x A(x'')dx'' \right] dx'. \qquad (3.8)$$

The results of some inversions are now shown. In all of the examples in this paper, synthetic $R^{\pm}$ data were generated using Eqs. (2.1) and (2.2), and T data were generated via Eq. (3.15) in Part I. The procedure for doing this was to first choose an $(\epsilon(z),\sigma(z))$ profile, convert to an $(A(x),B(x))$ profile, generate $R^{\pm}$ and T for two different step sizes (Δx), and then extrapolate those results to obtain the data for the inverse problem. The accuracy of all numerical algorithms was verified using the exact solutions displayed in Part I, Appendix B. All calculations were performed in single precision on a VAX 11/750.

Example 1: The (ϵ,σ) profiles in this example are approximately piecewise constant, as shown in Fig. 2. (Recall that the derivations required that ϵ be smooth.) The length of the medium is 10 m and permittivity relative to that of free space is shown. Scattering data for this medium are displayed in Fig. 3 for two round trips in the medium, although it is only the data for $0 < s < 2$ that are used in the inversion algorithm. It is difficult to see the discontinuities in $R^{\pm}(0,1,s)$ at $s = 2$. Figure 4 shows the resolvent kernel $W(0,1,s)$, which is obtained from Eq. (2.8). Notice the compact support, with W vanishing for $s > 2$. The $R^{\pm}$ data are shown differently in Fig. 5, with the R^{+} time scale running along the bottom axis and the R^{-} along the top. The spikes in the two time traces line up at corresponding regions of high reflectivity in the medium. Those traces decay toward zero quite rapidly due to the absorption of energy in the medium and the reflection of energy out of the medium.

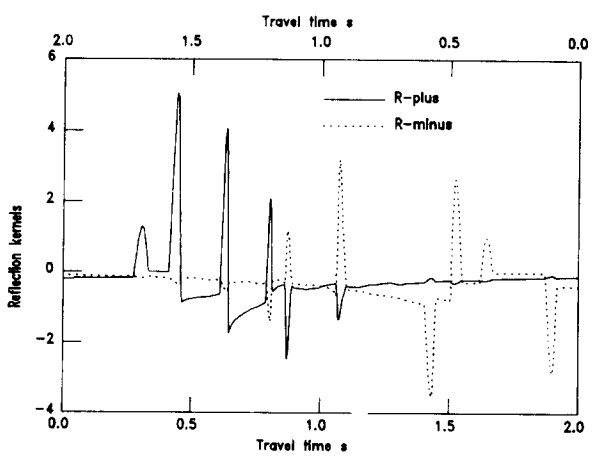

FIG. 5. The physical reflection kernels $R^{\pm}(0,1,s)$ for example 1 for one round trip. The solid line is the time trace for R^{+} and should be read from left to right using the lower scale in the figure. The dotted line shows R^{-} and should be read from right to left using the upper scale.

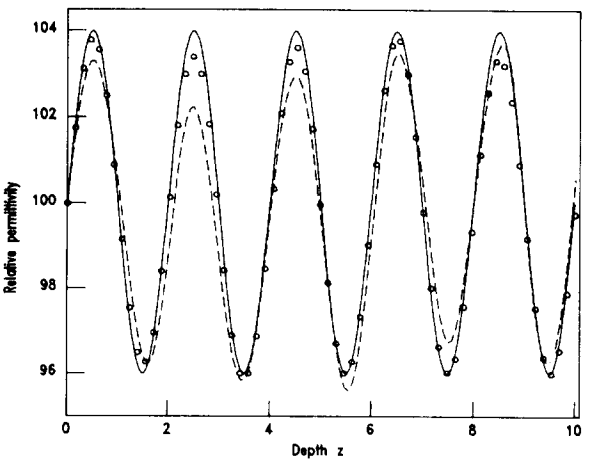

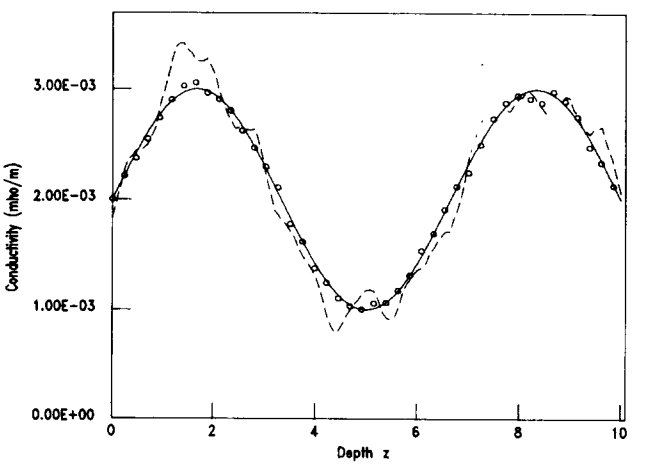

FIG. 6. The relative permittivity and conductivity profiles in example 2. The solid lines are the true profiles and the broken lines and the circles are reconstructions using noisy data. Each reconstruction uses 129 data points, but for graphical clarity not all circles are displayed. For an explanation of the noise, see the text. The depth is given in m.

The reconstructed profiles are shown in Fig. 2. These reconstructions used 513 data points from each of the time traces for $R^{\pm}$ and T. There is essentially no difference if 257 points are used instead.

Example 2: The performance of the inversion algorithm with noisy data is now examined. The medium profiles are shown by the solid lines in Fig. 6. The exact scattering data for these profiles are shown by the solid lines in Fig. 7. Gaussian white noise was then added to the kernels, resulting in

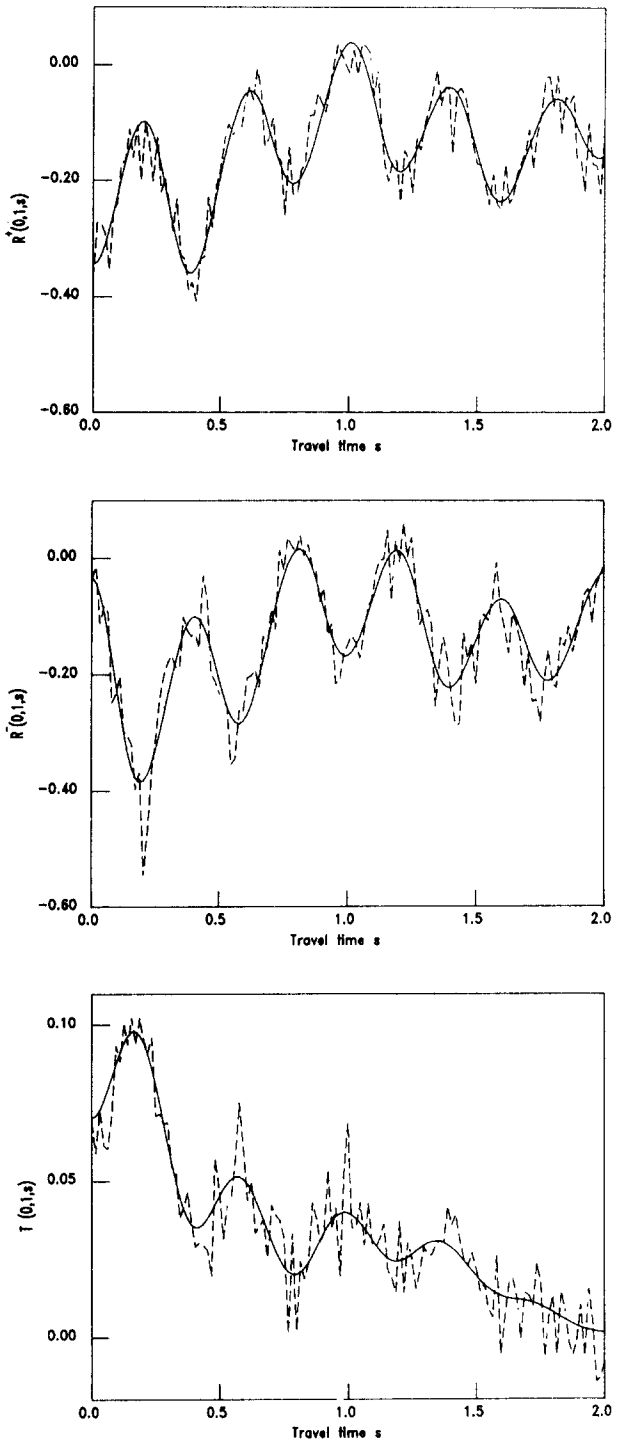

FIG. 7. The physical scattering kernels $R^{\pm}(0,1,s)$ and $T(0,1,s)$ for example 2. The solid lines are the time traces without noise and the broken lines show the noisy data with rms $S/N \doteq 1.8$. For further details, see the text.

the corrupted data shown by the broken lines in Fig. 7. The signal to noise ratio for these data is approximately 1.8. The noisy data were smoothed using two applications of a five point linear least squares smoother. (The first application left too much high-frequency noise in the data.) The broken line in Fig. 6 shows the resulting reconstructions using 129 data points. The reconstruction was carried out a second time with noisy data having signal to noise ratio of approximately 6.8. The results are much improved, and are shown with circles in Fig. 6. In the absence of noise, the reconstructed profiles are indistinguishable from the original profiles.

The definition of the root mean square signal to noise ratio (rms S/N) that was used above is

$$\text{rms } S/N = \left[\int_0^2 [K(0,1,s) - \bar{K}]^2 \, ds \right]^{1/2} \Big/ (2\sigma).$$

Here, σ denotes the standard deviation of the noise, $K(0,1,s)$ denotes a noisy scattering kernel, and

$$\bar{K} = \frac{1}{2} \int_0^2 K(0,1,s) ds.$$

IV. INVERSION USING REFLECTION DATA FROM BOTH INTERFACES

In the previous section an inversion algorithm was presented that utilized both of the reflection kernels and the transmission kernel for one complete round trip in the slab. These data are sufficient to recover both A and B (i.e., ϵ and σ) for the medium. In this section an inversion algorithm is given that uses only the reflection data $R^{\pm}(0,1,s)$ for a complete round trip. More explicitly, the data are a subset of (3.1), namely, $R^{\pm}(0,1,s)$, $0<s<2$, and constants l and $\epsilon(0)$ [or $\epsilon(L)$].

The algorithm is an iteration procedure. It has the property that the iterates may not converge, and if they do converge, the result may not be the correct solution. However, sufficient conditions for convergence to the correct solution are supplied in the Appendix.

The basis for the inversion algorithm is Eqs. (2.1) and (2.2). Begin by setting $y = 1$ in Eq. (2.1) and using the directional derivative nature of that equation to rewrite Eq. (2.1) in integrated form as

$$R^+(x,1,s) = R^+(0,1,s+2x) - \int_0^x \{B(x')R^+(x',1,s+2(x-x')) + \tfrac{1}{2}[A(x')+B(x')](R^+ * R^+)(x',1,s+2(x-x'))\} dx', \tag{4.1}$$

where the $*$ operation denotes convolution in s,

$$(f * g)(x,y,s) = \int_0^s f(x,y,s')g(x,y,s-s')ds'. \tag{4.2}$$

Similarly, in integrated form, Eq. (2.2) becomes (with $x = 0$)

$$R^-(0,y,s) = R^-(0,1,s+2(1-y)) - \int_y^1 \{B(y')R^-(0,y',s+2(y'-y)) - \tfrac{1}{2}[A(y') - B(y')](R^- * R^-)(0,y',s+2(y'-y))\}dy'. \tag{4.3}$$

Notice that the first term on the right-hand side of Eqs. (4.1) and (4.3) is the given reflection data. Denote this by

$$F^{\pm}(s) = R^{\pm}(0,1,s). \tag{4.4}$$

Now Eqs. (4.1) and (4.3) form the basis for an iteration procedure given by

$$R^+_{n+1}(x,1,s) = F^+(s+2x) - \int_0^x \{B_n(x')\,R^+_n(x',1,s+2(x-x')) + \tfrac{1}{2}[A_n(x') + B_n(x')](R^+_n * R^+_n)(x',1,s+2(x-x'))\}dx', \tag{4.5}$$

with $0 \leqslant x \leqslant 1$, $0 < s < 2(1-x)$, $n = 1, 2, 3, \ldots$, and

$$R^-_{n+1}(0,y,s) = F^-(s+2(1-y)) - \int_y^1 \{B_n(y')\,R^-_n(0,y',s+2(y'-y)) - \tfrac{1}{2}[A_n(y') - B_n(y')](R^-_n * R^-_n)(0,y',s+2(y'-y))\}dy', \tag{4.6}$$

with $0 \leqslant y \leqslant 1$, $0 < s < 2y$, and $n = 1, 2, 3, \ldots$. The functions A_n and B_n are defined as

$$A_n(x) = 2[R^-_n(0,x,0^+) - R^+_n(x,1,0^+)],$$
$$B_n(x) = 2[R^-_n(0,x,0^+) + R^+_n(x,1,0^+)], \tag{4.7}$$

which is suggested by the initial conditions given in Eqs. (2.1) and (2.2). One method for starting the iteration is to choose

$$R^+_1(x,1,s) = F^+(s+2x),$$
$$R^-_1(0,y,s) = F^-(s+2(1-y)). \tag{4.8}$$

Now if the iterates converge,

$$R^{\pm}_n \to R^{\pm}, \tag{4.9}$$

then it is natural to define $A(x)$ and $B(x)$ by Eq. (4.7), with subscript n removed from all quantities. Also, notice that if the iterates converge, then the limit functions given in Eq. (4.9) agree with the given reflection data when x is set equal to 0 and y is set equal to 1.

It is interesting to note that the initialization procedure given in Eq. (4.8) is a generalization of the nondissipative Bremmer approximation given in Ref. 12. It corresponds to ignoring dissipative effects on the reflected fields as well as ignoring multiple scattering effects. Hence, in a weakly dissipative, weakly scattering medium, Eqs. (4.7) and (4.8) themselves yield a good approximation to A and B given by

$$A(x) \doteq A_1(x) = 2[R^-_1(0,1,2(1-x)) - R^+_1(0,1,2x)],$$
$$B(x) \doteq B_1(x) = 2[R^-_1(0,1,2(1-x)) + R^+_1(0,1,2x)]. \tag{4.10}$$

Continuing the iteration can be thought of as bringing higher-order effects into the calculation.

Sufficient conditions exist to guarantee that the scheme

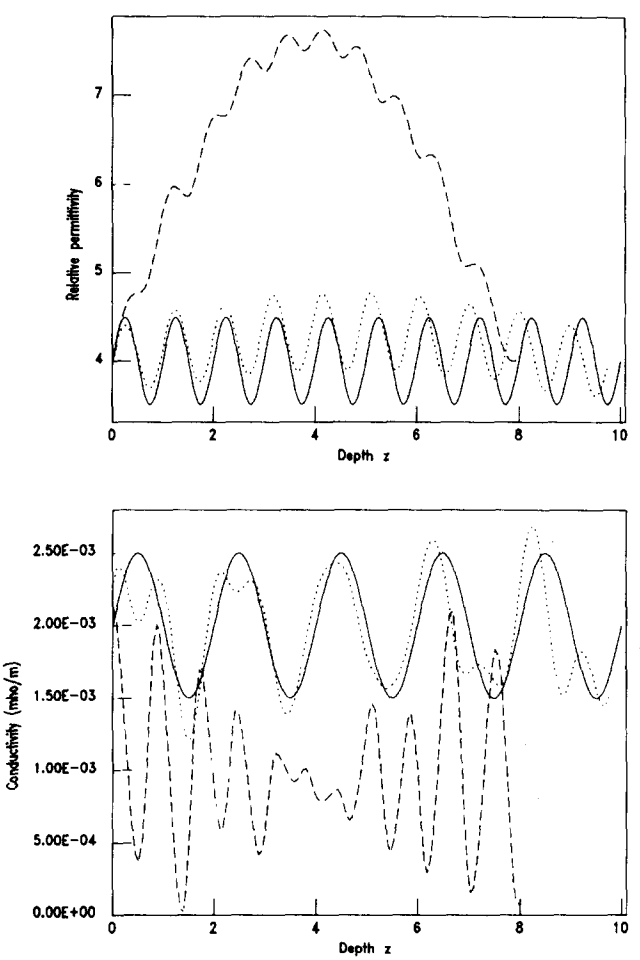

FIG. 8. The relative permittivity and conductivity profiles in example 3. The solid lines are the true profiles, and the broken lines are the initial approximations given by Eq. (4.10). The dotted lines show the profiles after 20 iterations. After 60 iterations the profiles coincide with the solid lines. The depth is given in m.

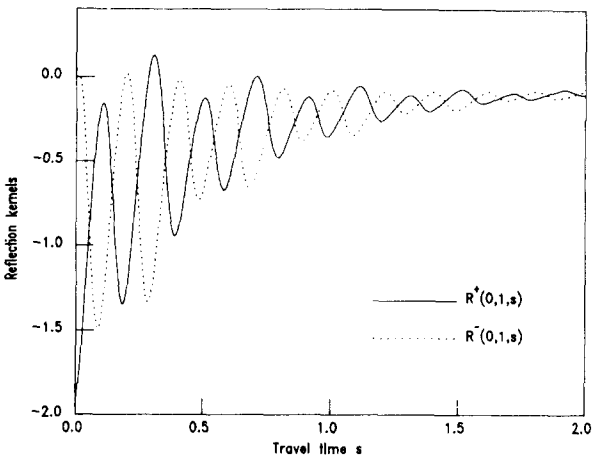

FIG. 9. The physical reflection kernels $R^{\pm}(0,1,s)$ for example 3.

does converge to one and only one solution. These are conditions on the physical reflection data and therefore have practical implication. The conditions are

$$|F^{\pm}(s)| < f, \quad 0 < s < 2, \tag{4.11}$$

where $f = (11/\sqrt{22} - 50)/27 \doteq 0.059\,06$. In the Appendix, it is shown that if the condition (4.11) is satisfied, then the solution of the inverse problem, (A,B), exists, is unique, and depends continuously on the data $F^{\pm}$. Thus, in this case, reflection data alone suffice to reconstruct A and B.

These positive results do not imply that any two functions $F^{\pm}$ satisfying (4.11) correspond to scattering data for some physical medium. This is because the reconstructed $B(x)$ may be greater than 0, a result that is nonphysical for the model problem, Eq. (2.1) in Part I. Also, condition (4.11) is not a necessary condition for convergence, as will be apparent from the following example.

Example 3: The ϵ and σ profiles are shown in solid lines in Fig. 8, and the corresponding $R^{\pm}$ data are shown in Fig. 9. Notice that these data do not satisfy condition (4.11). Nevertheless, the iterates converge to the original profiles in Fig. 8. The broken lines in Fig. 8 display the estimates of ϵ and σ given by the initialization procedure in Eqs. (4.8), or equivalently in Eqs. (4.10). After 20 iterations the estimates of ϵ and σ are given by the dotted lines in Fig. 8. After 60 iterations the estimates coincide with the original profiles. Continuing the iteration procedure produces no change in the estimated profiles.

V. INVERSION USING REFLECTION DATA FROM ONE INTERFACE

It was shown in the previous section that under certain circumstances, reflection data from both interfaces can be used to uniquely reconstruct A and B. In this section some aspects of reconstructing A and B are considered for the case in which the data consist only of $R^{+}(0,1,s)$ for $0 < s < 2$. This is an important problem since it corresponds to the case in which all data measurement is carried out on one side of the slab and consequently, a semi-infinite medium can be considered. In such a case, the parameter l defined in Part I, Eq. (2.6), is given by

$$l = t_{\max}/2, \tag{5.1}$$

where data is collected for physical time t in the interval $0 < t < t_{\max}$. Thus, only a finite portion of the medium can be probed, namely, that portion for $0 < z < L$, where L is given in Part I, Eq. (2.6), with l as in Eq. (5.1) above.

In this case it seems intuitively clear that nonunique solutions (A,B) should exist, provided the data correspond to a physical reflection kernel. The intuition here is that a single function of s (for $0 < s < 2$) cannot be used to reconstruct two independent functions $A(x)$, $B(x)$ for $0 < x < 1$.

If it is known *a priori* that the medium is nondissipative so that $B = 0$, then Eq. (2.1) can be used in an inversion algorithm to recover $A(x)$. This has been shown in Refs. 2 and 12. More generally, if the conductivity $\sigma(z)$ is known, then Eq. (2.1) can be used to recover the permittivity $\epsilon(z)$ or vice versa. Such problems have been considered in Refs. 2, 3, and 13. Integral equation methods for solving problems of this latter variety have been considered by Bolomey *et al.*[14] and Tijhuis.[15] It has also been shown by Corones *et al.*[2,3,13] that if the *a priori* information about conductivity (or permittivity) is incorrect, then the resulting reconstruction can degrade somewhat dramatically.

The question now addressed is, "What profiles pairs (A,B) [or (ϵ,σ)] produce the same one-sided reflection data, $R^{+}(0,1,s)$, for $0 < s < 2$?" A partial answer to this question will be given by considering media with "small" profile functions A and B. In this case the explicit dependence of the reflection data on A,B can be given asymptotically.

To carry this out, set $y = 1$ in Eq. (2.1) and again use the directional derivative nature of that equation to obtain for $0 < s < 2(1-x)$,

$$\begin{aligned} R^{+}(x,1,s) = {} & \tfrac{1}{4}[B(x+s/2) - A(x+s/2)] \\ & + \int_{x}^{x+s/2} \{B(x')R^{+}(x',1,s+2(x-x')) \\ & + \tfrac{1}{2}[A(x') + B(x')](R^{+} * R^{+}) \\ & (x',1,s+2(x-x'))\}dx'. \end{aligned} \tag{5.2}$$

This integrated form of Eq. (2.1) is well suited to the study of the direct problem, while Eq. (4.1) is better suited to the inverse problem. Now define a sequence of iterates given by

$$\begin{aligned} R_1(x,1,s) = {} & \tfrac{1}{4}[B(x+s/2) - A(x+s/2)], \\ R_{n+1}(x,1,s) = {} & \tfrac{1}{4}(B(x+s/2) - A(x+s/2)) \\ & + \int_{x}^{x+s/2} \{B(x')R_n(x',1,s+2(x-x')) \\ & + \tfrac{1}{2}[A(x') + B(x')](R_n * R_n) \\ & (x',1,s+2(x-x'))\}dx', \end{aligned} \tag{5.3}$$

where $n = 1,2,3,\ldots$. Define λ by

$$\lambda = \sup_{0<x<1} \{|A(x)|, |B(x)|\}.$$

For small λ it follows that the reflection data, $R^{+}(0,1,s)$, are

asymptotic to $R_2(0,1,s)$, with

$$R^+(0,1,s) \sim R_2(0,1,s)$$
$$= \frac{1}{4}\left(B\left(\frac{s}{2}\right) - A\left(\frac{s}{2}\right)\right)\left(1 + \int_0^{s/2} B(x')dx'\right)$$
$$+ O(\lambda^3), \lambda \to 0. \quad (5.4)$$

Thus, two profile pairs, (A_0, B_0) and (A_1, B_1), produce the same reflection data (asymptotically) for $0 < s < 2$ if

$$(B_0(x) - A_0(x))\left(1 + \int_0^x B_0(x')dx'\right)$$
$$= (B_1(x) - A_1(x))\left(1 + \int_0^x B_1(x')dx'\right). \quad (5.5)$$

Notice that it follows from Eq. (5.5) that $A_0 = A_1$ if and only if $B_0 = B_1$.

It is interesting to consider Eq. (5.5) for the special case involving a homogeneous, dissipative medium. Thus, assume that both $\epsilon(z)$ and $\sigma(z)$ are constants denoted by ϵ and σ, respectively. Then $A_0(x) \equiv 0$ and $B_0(x) = -\beta = -l\sigma/\epsilon$, where β is small. An equivalent, nondissipative scatterer is then obtained from Eq. (5.5) by setting $B_1(x) \equiv 0$ and solving for $A_1(x)$ [with corresponding permittivity $\epsilon_1(z)$]. This yields

$$A_1(x) = \beta(1 - \beta x), \quad 0 < x < 1, \quad (5.6)$$

and so, from Eqs. (3.5) and (3.6),

$$z(x) = \frac{l}{\sqrt{\epsilon\mu_0}} \int_0^x \exp\left[-\beta x'\left(1 - \frac{\beta x'}{2}\right)\right] dx', \quad (5.7)$$

$$\epsilon_1(z(x)) = \epsilon \exp\left[2\beta x(1 - \beta x/2)\right]. \quad (5.8)$$

Notice from Eq. (5.8) that $\epsilon_1(z)$ is an increasing function of z, while Eq. (5.7) shows that the depth L_1 of this equivalent medium has decreased from the original depth L_0 to

$$L_1 = L_0 \int_0^1 \exp\left[-\beta x'\left(1 - \frac{\beta x'}{2}\right)\right] dx'. \quad (5.9)$$

These conclusions are in agreement with the numerical results given in example 1 of Ref. 2, which suggest that equivalent scatterers that are obtained by decreasing σ result in an increasing permittivity profile and a more shallow medium.

VI. SUMMARY AND CONCLUSIONS

In Sec. III a new time domain inversion procedure for lossy media is developed. The algorithm uses the set of data given by (3.1). With the concept of "extension of data" developed in Part I, this set of data can be used to derive the entire time trace of the scattering kernels. However, data from only one round trip are explicitly used in the algorithm. The possibility of using longer time traces is not addressed in this paper.

At first sight it may seem a little surprising that three functions of time ($R^{\pm}$ and T) have to be given in order to obtain the two unknown functions $A(x)$ and $B(x)$ [or $\epsilon(z)$ and $\sigma(z)$]. It is, however, interesting to observe that other authors[4-8] use similar data sets to invert lossy profiles. The next example shows the importance of transmission data for reliable reconstructions when data from only one round trip are used.

Example 4: In this example it is shown that two different media can produce virtually identical $R^{\pm}$ reflection data for times less than one round trip through the slab, while at the same time producing different transmission data. The two different profiles are shown in Fig. 10 and the corresponding scattering data are given in Fig. 11. The dotted line profile was found by the iteration scheme presented in Sec. IV. It is seen that reflection data are virtually identical up to one round trip. At later times the reflection data are different as well as their discontinuities at one round trip. The transmission data, however, are different for all times. The two profiles are thus equivalent in that they are indistinguishable by just using reflection data for times less than one round trip. Consequently, transmission data are necessary (in general) for reliable reconstructions.

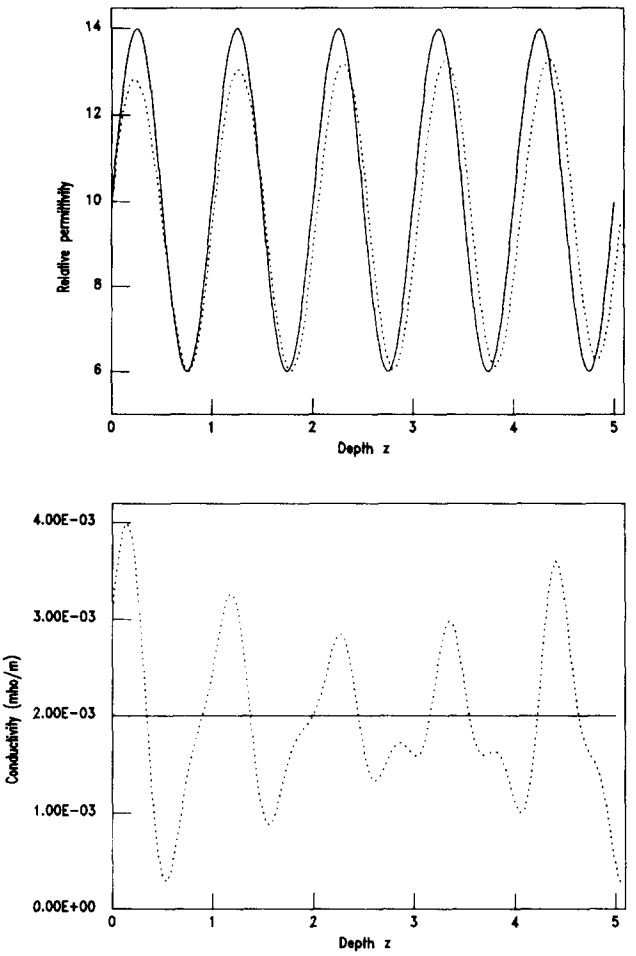

FIG. 10. The relative permittivity and conductivity in example 4. The depth is given in m.

An iterative inversion scheme using only reflection data for one round trip is presented in Sec. IV. The limitations of this inversion algorithm are illustrated by the example in this section. However, sufficient conditions for convergence of the iteration scheme are derived in the Appendix. Notice that this scheme is much more computer intensive than that of Sec. III, with one step of the iteration taking as long as the entire inversion procedure when transmission data are also available.

The effect of using reflection data from one side only is

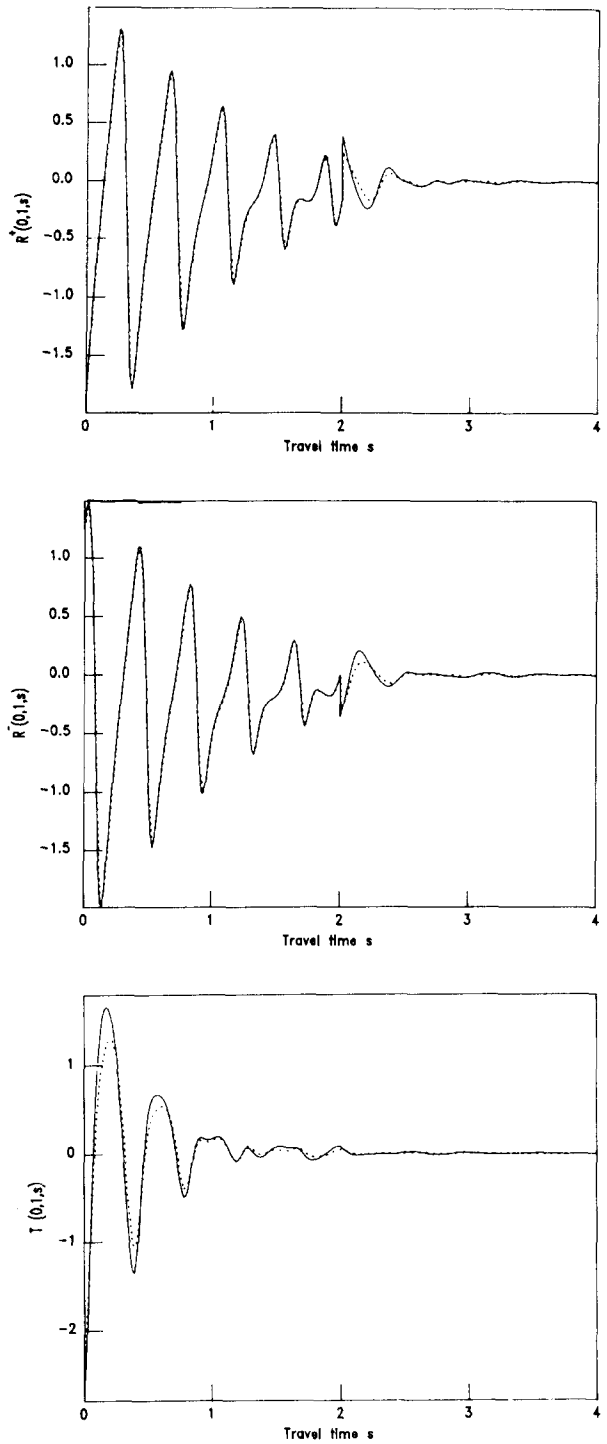

FIG. 11. The physical scattering kernels $R^{\pm}(0,1,s)$ and $T(0,1,s)$ for example 4. Two round trips are shown. The solid (dotted) lines correspond to the solid (dotted) line profiles in Fig. 10.

discussed in Sec. V. It is shown that for weakly scattering media (in which only the lowest-order multiple scattering effects are important), an entire family of media can be generated that produce the same one-sided reflection data for one round trip in travel time. In particular, this implies that for a semi-infinite medium, it is impossible to determine both $\epsilon(z)$ and $\sigma(z)$ from reflection data using normal incidence.

ACKNOWLEDGMENTS

This work was performed at Ames Laboratory, U. S. D. O. E., Iowa State University, and was supported by the Applied Mathematical Sciences subprogram of the Office of Energy Research, U. S. Department of Energy, under Contract No. W-7405-ENG-82, and by the Office of Naval Research Contract No. N0014-83-K-0038. One of the authors (G. K.) would like to thank Ames Laboratory for their hospitality during his visit in the United States. He is also grateful to the National Swedish Board for Technical Development (STUF) for partial support.

APPENDIX: CONVERGENCE OF THE ITERATION PROCEDURE

This appendix shows an analysis of the iteration procedure given in Sec. IV. In particular, it is shown that the condition in Eq. (4.11) guarantees the convergence of the iterates, the uniqueness of the solution and the continuous dependence of the solution on the data $F^{\pm}$.

To begin, suppose the reflection data are bounded by a constant f over one round trip in the slab, i.e.,

$$|F^{\pm}(s)| \leqslant f, \quad 0 < s < 2. \tag{A1}$$

Does it follow that all the iterates $R_n^{\pm}$, given in Eqs. (4.5) and (4.6), are uniformly bounded? Assume there is a constant b such that, for all n,

$$\begin{aligned} &|R_n^{+}(x,1,s)| \leqslant b, \quad 0 \leqslant x \leqslant 1, \quad 0 < s < 2(1-x), \\ &|R_n^{-}(0,y,s)| \leqslant b, \quad 0 \leqslant y \leqslant 1, \quad 0 < s < 2y. \end{aligned} \tag{A2}$$

In this case, it follows that

$$\begin{aligned} &|A_n(x) + B_n(x)| = 4|R_n^{-}(0,x,0^{+})| \leqslant 4b, \\ &|B_n(x)| \leqslant 4b, \end{aligned} \tag{A3}$$

from Eqs. (4.7). Consequently, from Eq. (4.5) it is seen that

$$\begin{aligned} |R_{n+1}^{+}(x,1,s)| &\leqslant f + 4b^2 x + 2b^3 x(s+x) \\ &\leqslant f + 4b^2 + 2b^3, \end{aligned} \tag{A4}$$

for $0 \leqslant x \leqslant 1$, $0 < s < 2(1-x)$. Similarly, it can be shown that

$$|R_{n+1}^{-}(0,y,s)| \leqslant f + 4b^2 + 2b^3, \tag{A5}$$

for $0 \leqslant y \leqslant 1$, $0 < s < 2y$. In order to satisfy the uniform bound on the iterates given in Eq. (A2), it therefore suffices to require that

$$f + 4b^2 + 2b^3 \leqslant b. \tag{A6}$$

The object is to now choose the largest value of f such that a positive b exists which satisfies Eq. (A6) and therefore Eq. (A2). This occurs when

$$8b + 6b^2 = 1 \tag{A7}$$

or

$$b = b_0 = (\sqrt{22} - 4)/6 \doteq 0.115\,07, \tag{A8}$$

and consequently

$$f = f_0 = (11\sqrt{22} - 50)/27 \doteq 0.059\,06. \tag{A9}$$

Having shown that it is possible for the iterates to remain uniformly bounded, it now must be demonstrated that the iterates actually converge. This follows from the contraction mapping principle, or equivalently from a comparison

of successive iterates. To see this, assume

$$|F^{\pm}(s)| \leqslant f_1 < f_0, \quad 0 < s < 2, \tag{A10}$$

so that

$$|R_n^{+}(x,1,s)|, |R_n^{-}(0,y,s)| \leqslant b_1 < b_0$$

in the appropriate triangular regions. Define for $n = 1,2,\ldots$ (with $R_0^{\pm} \equiv 0$)

$$c_n = \sup_{(x,y,s)} [|R_n^{+}(x,1,s) - R_{n-1}^{+}(x,1,s)|, \; |R_n^{-}(0,y,s) - R_{n-1}^{-}(0,y,s)|], \tag{A11}$$

with arguments x, y, s in the relevant domains. Now from Eq. (4.5) it follows that

$$\begin{aligned} |R_{n+1}^{+}(x,1,s) - R_n^{+}(x,1,s)| \leqslant \int_0^x & |B_n(R_n^{+} - R_{n-1}^{+}) + R_{n-1}^{+}(B_n - B_{n-1}) \\ & + 2R_n^{-}(0,x',0^{+})[R_n^{+} * R_n^{+} - R_{n-1}^{+} * R_{n-1}^{+}] \\ & + 2[R_n^{-}(0,x',0^{+}) - R_{n-1}^{-}(0,x',0^{+})](R_{n-1}^{+} * R_{n-1}^{+})|dx' \leqslant kc_n \end{aligned} \tag{A12}$$

where

$$k = 8b_1 + 6b_1^2 < 1, \tag{A13}$$

this last inequality following from the fact that $b_1 < b_0$. [In Eq. (A12) the $*$ denotes convolution in s and the suppressed arguments in B_n and the R^{+} iterates are x' and $(x',1,s + 2(x - x'))$, respectively.] Similarly, it can be shown that

$$|R_{n+1}^{-}(0,y,s) - R_n^{-}(0,y,s)| \leqslant kc_n,$$

and consequently

$$c_{n+1} \leqslant kc_n.$$

Hence, the iteration converges since $k < 1$. Standard arguments now show that if Eq. (A10) is satisfied, then the iteration converges to a unique limit as long as the initial iterates $R_1^{\pm}$ are bounded by $b_1 < b_0$.

Finally, to show continuous dependence on the scattering data, suppose two sets of reflection data $F^{\pm}$ and $\tilde{F}^{\pm}$ both satisfy Eq. (A10) and

$$|F^{\pm}(s) - \tilde{F}^{\pm}(s)| < \epsilon.$$

Denote the corresponding iterates by $R_n^{\pm}$ and $\tilde{R}_n^{\pm}$. All of these iterates are uniformly bounded by some $b_1 < b_0$. Define

$$d_n = \sup_{(x,y,s)} [|R_n^{+}(x,1,s) - \tilde{R}_n^{+}(x,1,s)|, \; |R_n^{-}(0,y,s) - \tilde{R}_n^{-}(0,y,s)|], \tag{A14}$$

with x, y, s in the appropriate domains. Using Eq. (4.5) with each set of data then yields [in a manner similar to that in which Eq. (A12) was derived]

$$|R_{n+1}^{+}(x,1,s) - \tilde{R}_{n+1}^{+}(x,1,s)| < \epsilon + kd_n,$$

where k is given by Eq. (A13). Consequently, it can be shown that

$$d_{n+1} \leqslant \epsilon + kd_n. \tag{A15}$$

Since $d_1 < \epsilon$ it follows from (A15) that

$$d_n \leqslant \epsilon \sum_{j=0}^{n-1} k^j < \frac{\epsilon}{1-k},$$

for $n = 1,2,\ldots$. Hence,

$$|A(x) - \tilde{A}(x)| < 4\epsilon/(1-k),$$
$$|B(x) - \tilde{B}(x)| < 4\epsilon/(1-k),$$

where $k < 1$. This established the continuous dependence of A and B on the scattering data.

[1] G. Kristensson and R. J. Krueger, "Direct and inverse scattering in the time domain for a dissipative wave equation. Scattering operators," J. Math. Phys. **27**, 1667 (1986).

[2] J. P. Corones, M. E. Davison, and R. J. Krueger, "The effects of dissipation in one-dimensional inverse problems," in *Inverse Optics, Proceedings of the SPIE*, Vol. 413, edited by A. J. Devaney (SPIE, Bellingham, WA, 1983), pp. 107–114.

[3] J. P. Corones, M. E. Davison, and R. J. Krueger, "Dissipative inverse problems in the time domain," in *Inverse Methods in Electromagnetic Imaging*, NATO ASI series, Series C, Vol. 143, edited by W-M. Boerner (Reidel, Dordrecht, 1985), pp. 121–130.

[4] M. Jaulent, "Inverse scattering problems in absorbing media," J. Math. Phys. **17**, 1351 (1976).

[5] M. Jaulent, "Inverse scattering problem for LCRG transmission lines," J. Math. Phys. **23**, 2286 (1982).

[6] V. Weston, "On the inverse problem for a hyperbolic dispersive partial differential equation," J. Math. Phys. **13**, 1952 (1972).

[7] V. Weston and R. J. Krueger, "On the inverse problem for a hyperbolic dispersive partial differential equation. II," J. Math. Phys. **14**, 406 (1973).

[8] V. Weston, "On inverse scattering," J. Math. Phys. **15**, 209 (1974).

[9] R. J. Krueger, "An inverse problem for a dissipative hyperbolic equation with discontinuous coefficients," Quart. Appl. Math. **34**, 129 (1976).

[10] R. J. Krueger, "An inverse problem for an absorbing medium with multiple discontinuities," Quart. Appl. Math. **36**, 235 (1978).

[11] R. J. Krueger, "Numerical aspects of a dissipative inverse problem," IEEE Trans. Antennas Propag. **AP-29**, 253 (1981).

[12] J. P. Corones, M. E. Davison, and R. J. Krueger, "Direct and inverse scattering in the time domain via invariant imbedding equations," J. Acoust. Soc. Am. **74**, 1535 (1983).

[13] J. P. Corones, R. J. Krueger, and V. H. Weston, "Some recent results in inverse scattering theory," in *Inverse Problems of Acoustic and Elastic Waves*, edited by F. Santosa, Y. Pao, W. Symes, and C. Holland (SIAM, Philadelphia, PA, 1984), pp. 65–81.

[14] J. C. Bolomey, D. Lesselier, C. Pichot, and W. Tabbara, "Spectral and time domain approaches to some inverse scattering problems," IEEE Trans. Antennas Propag. **AP-29**, 206 (1981).

[15] A. G. Tijhuis, "Iterative determination of permittivity and conductivity profiles of a dielectric slab in the time domain," IEEE Trans. Antennas Propag. **AP-29**, 239 (1981).